Chemistry–A European Journal
Research Article
doi.org/10.1002/chem.202301634
Chemistry Europe
European Chemical Societies Publishing
www.chemeurj.org

Hot Paper

Highly Efficient Oxindole-Based Molecular Photoswitches

Daniel Doellerer,[a] Daisy R. S. Pooler,[a] Ainoa Guinart,[a] Stefano Crespi,*[a, b] and Ben L. Feringa*[a]

3-Benzylidene-indoline-2-ones play a prominent role in the pharmaceutical industry due to the diverse biomedical applications of oxindole heterocycles. Despite the extensive reports on their biological properties, these compounds have hardly been studied for their photochemical activity. Here, we present 3-benzylidene-indoline-2-ones as a promising class of photoswitches with high yields, robust photochemical switching with quantum yields reaching up to 50% and potential for biological applications.

Introduction

Bistable photoswitches undergo reversible photochromism between two distinct structures, through isomerization powered by light.[1,2] Prominent families of photochromic molecules include azobenzenes,[2] stiff-stilbenes,[3] spiropyrans,[4] and diarylethenes.[5] They have attracted tremendous attention in recent years as non-invasive molecular control units and have been implemented in numerous responsive systems, ranging from smart materials,[6] liquid crystals,[7] and energy storage[8] to photopharmacology.[9] Various opportunities to design responsive molecular systems and materials have stimulated the search for novel, broadly applicable photoswitches showing good reversibility and ease of functionalization. Recently, photoswitches based on heterocyclic dyes such as indigo,[10,11] hemithioindigo[12,13] and isoindigo[14] have been investigated, showing robust photochemical switching at red-shifted wavelengths – tackling the challenge of switching within the phototherapeutic window.[3,15,16]

Isoindigo is the self-condensation product of indoline-2-one, also known as oxindole, which is a privileged scaffold in organic synthesis. Oxindole and its derivatives are compounds of major biological and medicinal interest, and can be commonly found in a variety of natural products.[17,18a] In particular, functionalized 3-benzylidene-indoline-2-ones have found widespread application in the pharmaceutical industry for their anti-cancer, -bacterial, -fungal, -viral and -angiogenic properties.[18] Oxindole is a chromophore responsive to visible light which can be readily functionalized,[17] and has found photochemical applications as photosensitizers,[19] in photovoltaics[20] and more recently by our group, in the design of novel visible light-driven molecular motors.[21] However, despite the distinct features and interesting photochemical properties of oxindole and its potential for application in photopharmacology, its use as a scaffold within bistable photoswitches is hardly explored.[22]

Here, we introduce a family of conveniently accessible oxindole-based bistable photoswitches via a Knoevenagel condensation, with functionalization in the *ortho*-, *meta*- and *para*-positions of the benzylidene moiety. The effect of *N*-functionalization on the amide with either a methyl or phenyl group is also investigated. These novel molecular photoswitches show i) robust photochemical switching in the visible region of the electromagnetic spectrum, ii) backswitching behavior with light of a higher wavelength (470 nm) and iii) that it is possible to operate these switches (**3a-*E***, **3d-*E***, **3i-*E***, **3q-*E*** and **3u-*E***, see below) within liposomes, making them promising candidates for future biological applications.

Results and Discussion

All photoswitches were synthesized via a Knoevenagel condensation of oxindole with a range of benzaldehydes (**1a**–**1u**), facilitated by piperidine, where the yields range from moderate to excellent (Scheme 1). For the synthetic procedures and full characterization of all compounds, see Supporting Information. Different substitution patterns of the benzaldehyde fragment were introduced to investigate the steric and electronic effects, as well as the functional group tolerance. A complete substitution pattern of both electron-withdrawing fluoride (**3b-*E***–**3g-*E***) and -donating methoxy (**3h-*E***–**3m-*E***) groups at the phenyl ring was synthesized, including *ortho*-, *meta*- and *para*-substitutions, and combinations thereof. In addition, several di-*ortho* substituted switches are included (**3n-*E***–**3p-*E***) to exclude Mallory photocyclization as observed in the case of stilbenes.[23] Various para-substituted photoswitches (**3q-*E***–**3u-*E*** and **3q-*Z***) containing strongly electron-donating and -withdrawing groups were prepared, to probe electronic effects on the photo-

[a] D. Doellerer, Dr. D. R. S. Pooler, A. Guinart, Dr. S. Crespi, Prof. Dr. B. L. Feringa
Stratingh Institute for Chemistry
University of Groningen, Nijenborgh 4
9747 AG Groningen (The Netherlands)
E-mail: stefano.crespi@kemi.uu.se
b.l.feringa@rug.nl

[b] Dr. S. Crespi
Department of Chemistry – Ångström Laboratory, Uppsala University
Box 523, 751 20 Uppsala (Sweden)

Supporting information for this article is available on the WWW under https://doi.org/10.1002/chem.202301634

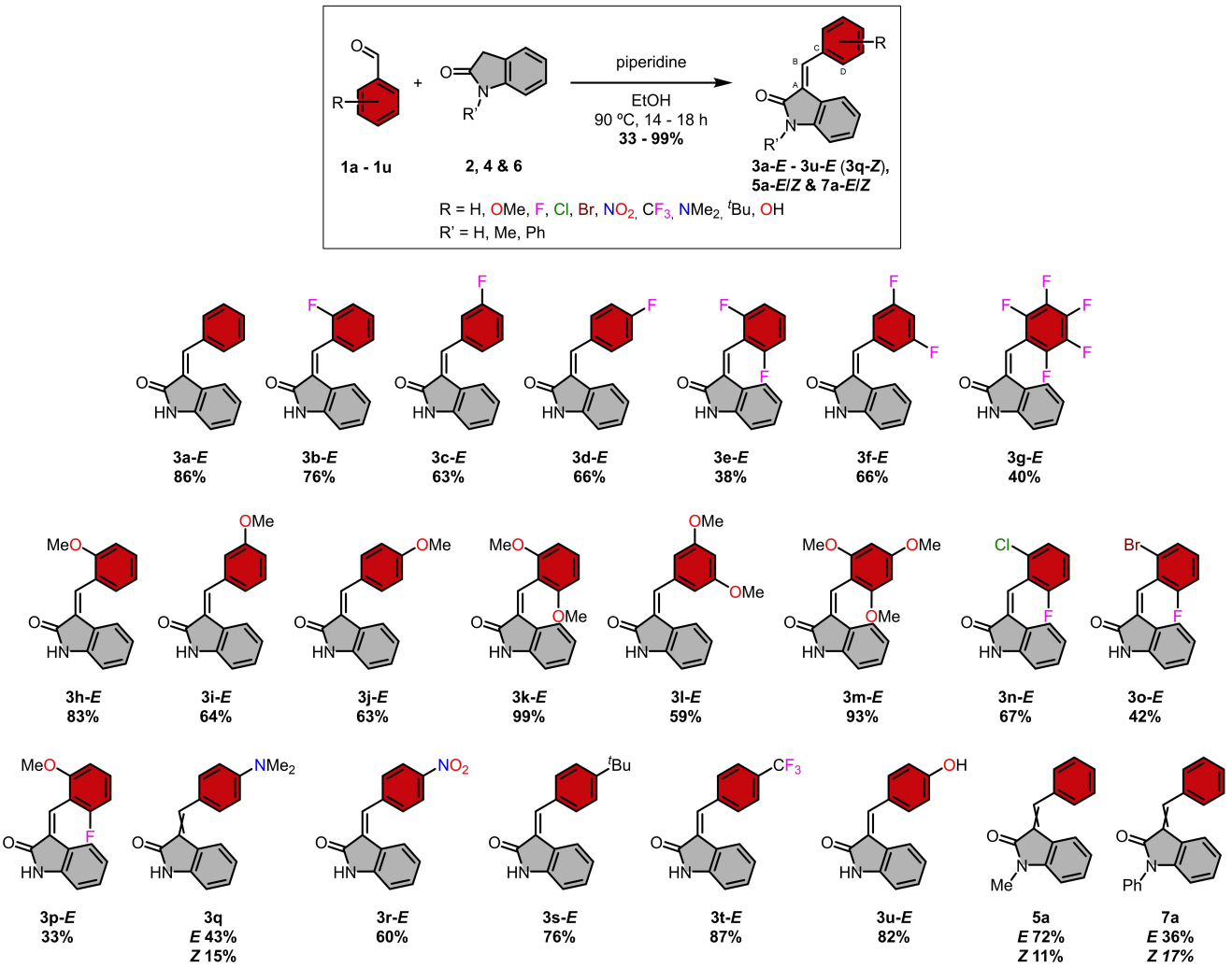

Scheme 1. Synthetic procedure to obtain switches **3a-*E*–3u-*E*** (**3q-*Z***), **5a-*E*/*Z*** and **7a-*E*/*Z*** (ABCD discussed dihedral angle; isolated yields).

switching. Finally, switches with methyl and phenyl substitutions at the oxindolic amide (**5a-*E*/*Z*** and **7a-*E*/*Z***, respectively) were made to compare with the parent compound **3a-*E***, to examine the effect of amide substitution on the photochemical properties.

The synthesized switches were initially studied by DFT calculations to predict their structural parameters and absorption spectra. All structures were optimized at the ωB97X–D/def2-SVP level in both the gas-phase and in acetonitrile using the SMD solvation model.[24] For the optimized structures of the *E* isomer in all of the switches, the phenyl ring is twisted out of plane with respect to the oxindole moiety, due to steric hindrance. Conversely in the *Z* isomer, the molecule is completely planar for most switches, however for those with *ortho*-substitution the phenyl ring is twisted out of planarity, due to steric hindrance between the amide group and the *ortho*-substituents. Their DFT calculated UV-Vis spectra show an intense π-π* absorption band (λ_{MAX} = ~300–350 nm) characterized by a red-shifted shoulder tailing up to 500 nm (see Supporting Information). The absorption maximum of compound **3r-*E*** with the most electron-withdrawing group (*para*-NO_2, $\sigma_p = +0.78$)[25] is around 340 nm for the π-π* band, and the shoulder centers around 430 nm. Conversely, the absorption maximum of compound **3q-*E*/*Z*** with the most electron-donating group (*para*-NMe_2, $\sigma_p = -0.83$)[25] is red-shifted by 80 nm to around 420 nm, almost fully depleting the band tailing into the visible region. This finding demonstrates the electronic effect of a push-pull system between the highly electron-donating benzylidene fragment with the electron-withdrawing oxindolic amide unit. Similar depletion of the second band is observed in photoswitch **3u-*E***, with the highly electron-donating hydroxyl group in the *para*-position ($\sigma_p = -0.37$).[25]

All isolated di-*ortho*-substituted molecules give lower yields except **3k-*E*** and **3m-*E***, which show almost quantitative yields. To better understand these exceptions and get an indication as to why this was the case, the computed dihedral angles (angle ABCD, Scheme 1) in CH_3CN of the di-*ortho*-substituted molecules (**3e-*E***, **3g-*E***, **3k-*E***, **3m-*E*–3p-*E***) were compared with each other. The calculated values range between 40–55° for most cases, therefore not providing any steric indication for the almost quantitative yields of **3k-*E*** and **3m-*E***. Nevertheless, it is

worth mentioning that the calculated dihedral angles of the *ortho*-substituted molecules are higher than non-/*meta*-/*para*-substituted molecules (50° compared to roughly 40–45°), because the substituted phenyl ring is twisted more out of planarity in comparison to the oxindole ring. The largest dihedrals were observed for **3n-*E*** and **3o-*E*** (66° and 74°, respectively), possibly due to the increased steric demand of their bulkier halogen substituents. All molecules were solely obtained as the more stable *E* isomer, except the *para*-dimethylamine substituted switch **3q** and the amide functionalized switches **5a** and **7a** (*E*:*Z* ratios being ~3:1, ~6.5:1 and ~2:1 for **3q**, **5a** and **7a** respectively). The isolation of **3q** as both its *E* and *Z* isomers is backed up with the performed DFT calculations, which show that the *Z* isomer of **3q** is more stable in the gas phase ($\Delta G_{calc} = -0.31$ kcal mol^{-1}) and acetonitrile ($\Delta G_{calc} = -0.32$ kcal mol^{-1}) in this case. The isolation of **3q-*Z*** has also been reported previously in the literature (Scheme 1).[26] The relative energies of both the *E* and *Z* optimized structures of all switches, as well as the energy barriers for the thermal *E*/*Z* isomerizations can be found in the Supporting Information (Table S4; measured thermal stability up to 70 °C for selected compounds, Figure S69, S74, S97). Note, based on this data and the calculations the compounds have thermal half-lives in the range of thousands of years at room temperature.

The photochemical properties and photoisomerization of all switches were investigated by NMR (^{1}H NMR and ^{19}F NMR) and UV-Vis spectroscopy (see Table 1 and Supporting Information). All compounds showed switching behavior when irradiated at 365 nm and their photostationary state (PSS) ratios could be determined by ^{1}H NMR in CD_3CN at 25 °C (see Table 1 and Supporting Information, Table S1). The only exception here was **3q-*E*/*Z***, which due to the highly electron-donating dimethylamine moiety was irradiated at 420 nm, since almost no change occurred with 365 nm light as a result of near identical absorptions of *E* and *Z* isomers at this wavelength. Due to the overlapping of key signals, integration of the signals for the *E* and *Z* isomers was not feasible by ^{1}H NMR for **3f-*E***, **3g-*E*** and **3n-*E***. In these cases, the switching behavior was analyzed by ^{19}F NMR (see Table 1 and Supporting Information). Some switches showed photostationary state ratios enriched in the metastable isomer, like **3c-*E***, **3l-*E***, **5a-*E*** and **7a-*E***, with below 30 % of the *E* isomer left at PSS.

All *ortho*-substituted photoswitches generate an almost 1:1 mixture of *E* and *Z* isomers at PSS, hence showing smaller relative differences in their UV-Vis absorption spectra (see

Table 1. Molar extinction coefficients at 20 °C in CH_3CN at 365 nm, PSS obtained upon irradiation with a 365 nm LED (420 nm LED for **3q-*E***) and QYs for switches **3a-*E*–3u-*E***, **5a-*E*** and **7a-*E***. Switches **3e-*E***, **3g-*E***, **3n-*E*** and **3o-*E*** showed no change in the UV-Vis spectra and thus no QY was determined. Switch **3f-*E*** did not reach a PSS in 200 min.

Entry	Compound	$\varepsilon_{(E)}$ [M^{-1} cm^{-1}]	$\varepsilon_{(Z)}$ [M^{-1} cm^{-1}]	PSS_{365} (*E*:*Z*)	QY [%] *E*→*Z*	QY [%] *Z*→*E*
1	**3a-*E***	4200	7100	31:69	9.9	2.7
2	**3b-*E***	2700	6850	56:44	13.0	0.7
3	**3c-*E***	3350	5650	10:90	2.4	0.1
4	**3d-*E***	4100	6600	34:66	23.6	7.7
5	**3e-*E***	–	–	45:55	–	–
6	**3f-*E***[a]	2550	3950	32:68	0.1	0.02
7	**3g-*E***	–	–	45:55	–	–
8	**3h-*E***	9000	14650	60:40	13.7	12.7
9	**3i-*E***	5250	12900	32:68	8.6	1.7
10	**3j-*E***	11400	19150	61:39	31.8	29.4
11	**3k-*E***	4400	6250	44:56	26.6	14.7
12	**3l-*E***	4250	8200	29:71	9.5	2.0
13	**3m-*E***	15500	16600	45:55	16.5	12.9
14	**3n-*E***	–	–	50:50	–	–
15	**3o-*E***	–	–	41:59	–	–
16	**3p-*E***	4250	5200	55:45	7.8	7.8
17	**3q-*E***[b]	27150	29700	53:47	12.7	12.6
18	**3r-*E***	8550	16650	74:26	1.7	2.5
19	**3s-*E***	6750	12800	58:42	21.2	15.8
20	**3t-*E***	2750	4100	65:35	0.1	0.1
21	**3u-*E***	12900	13650	40:60	49.7	30.4
22	**5a-*E***	2050	4250	22:78	4.6	0.6
23	**7a-*E***	2700	7800	22:78	11.9	1.1

[a] Did not reach PSS in 200 min. [b] Irradiated with a 420 nm LED.

Table 1 and Supporting Information, Table S2). Notably, the nature of the substituent at the amide moiety has little or no influence on the switching behavior, resulting in almost identical PSS ratios for **3a-*E*/*Z***, **5a-*E*/*Z*** and **7a-*E*/*Z*** (see Table 1 and Supporting Information).

We show molecule **7a-*E*/*Z*** as a representative example of the photochemistry of these switches, since it was isolated as both *E* and *Z* stereoisomers. When irradiating solutions of both, pure *E* and pure *Z* isomer of **7a** in CD_3CN at 365 nm, identical ^1H spectra and PSS ratios (*E*:*Z* = ~20:80) were obtained, showing switching from *E* to *Z* is more efficient, rather than *vice versa* (Figure 1; see Supporting Information for spectra of **3q-*E*/*Z*** and **5a-*E*/*Z***).

Once the PSS ratios were obtained using NMR spectroscopy, all switches were analyzed by UV-Vis (see Table 1 and Supporting Information). Interestingly, the UV-Vis spectra of non-*ortho* substituted switches show a larger increase in absorbance upon switching to PSS, due to the large conformational change upon formation of the *Z* isomer.

The spectra of di-*ortho*-substituted switches **3e-*E***, **3g-*E***, **3n-*E*** and **3o-*E***, however, did not change during irradiation to PSS, meaning that the *E* and *Z* isomers must have similar molar absorptivity coefficients at 365 nm. A possible explanation for this observation could be that both *E* and *Z* isomers have phenyl rings that are twisted out of plane with respect to the rest of the molecule, due to the steric demand of the halogen *ortho*-substituents, which is supported by the dihedral angles of the optimized structures. As mentioned before, the influence of amide substitution on the photophysical properties is negligible.

Compound **7a-*E*/*Z*** was investigated, where the absorbance starting from the *E* isomer increases upon irradiation due to a gain in planarity and decreases, in the case of the *Z* isomer, due to a loss in planarity. The spectra after irradiation to PSS from both the pure *E* and *Z* isomers of **7a** show an identical shape, again proving that the switching from both isomers reaches the same PSS (Figure 2; see Supporting Information for spectra of **3q-*E*/*Z*** and **5a-*E*/*Z***). Furthermore, fatigue studies were performed with switches **3a-*E***, **3d-*E*** and **7a-*E***, because these have the largest difference in absorption reaching PSS between *E* and *Z* isomer (Figure 2; see Supporting Information for spectra of **3a-*E*** and **3d-*E*** and NMR data concerning back-switching of **3a-*E***, **3d-*E*** and **7a-*E***). Switching from the photochemically generated *Z* isomer back to the *E* isomer was achieved fastest by irradiation using a 470 nm LED, although partial photochemical back-switching was also observed at a slower rate by using 445 and 505 nm LEDs.

Having both the PSS ratios from the NMR and concentrations from the UV-Vis measurements in hand, the quantum yield (QY) of the individual molecules could be determined using the method of Stranius and Börjesson,[27] (see Table 1 and Supporting Information, Table S2). *Para*-substituted molecules like **3d-*E***, **3j-*E***, **3k-*E***, **3s-*E*** and **3u-*E*** have higher quantum yields in comparison to the other investigated switches, reaching above 20% for the *E*→*Z* isomerization. Compounds **3j-*E***, **3k-*E***, **3m-*E***, **3s-*E*** and **3u-*E*** show moderate to high QY from *Z*→*E* as well, with **3j-*E*** and **3u-*E*** boosting the highest overall QYs for isomerization in both directions. On the other hand, the switches with highly electron-withdrawing groups in the *para*-position **3r-*E*** (*para*-NO_2) and **3t-*E*** (*para*-CF_3) do not follow this trend showing lower QYs for both isomerizations, possibly due to the electronic pull-pull system with the oxindolic amide group.[28] In addition, switches **3c-*E*** and **3f-*E*** also show very low QYs, where the QY of **3f-*E*** has to be considered with care since PSS was not reached after 200 min (Table 1 and Table S2). The QY for di-*ortho*-substituted switches **3e-*E***, **3g-*E***, **3n-*E*** and **3o-*E*** could not be determined since the obtained molar absorptivity coefficients of the *E* and *Z* isomers showed no significant difference, hence their spectral change at 365 nm was almost negligible. This finding may be due to the higher twist within the *Z* isomer. Comparison of **3a**, **5a** and **7a** shows, that **3a** and **7a** have almost identical QY values, whereas **5a** has slightly lower values (see Table 1 and Supporting Information).

The phenol functionalized molecular switch **3u-*E*** was investigated regarding its acid-base effect on the switching behavior, since the hydroxy group in *para*-position ($\sigma_p = -0.37$)[25] can be deprotonated readily. Deprotonation should shift the absorbance further towards the red since its functional group becomes a stronger electron donating group ($\sigma_p = -0.81$),[25] increasing the push-pull character of the switch. Thus, the effect of *in situ* addition of KOH to **3u-*E*** in MeOH was investigated via UV-Vis spectroscopy (20 °C, 365 nm LED). Indeed, the maximum absorption of **3u-*E*** was shifted by ~80 nm towards the red (352–429 nm) while still retaining its switching behavior when irradiated with a 365 nm LED (see Supporting Information, Figure S94). Next, a second aliquot of

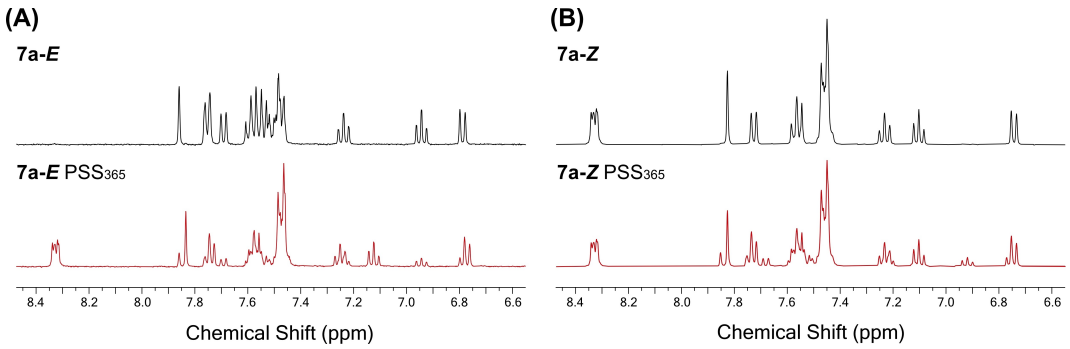

Figure 1. ^1H NMR spectra of A) **7a-*E***, black = initial spectrum, red = PSS_{365} – 22:78 (**7a-*E*:7a-*Z***) and B) **7a-*Z***, black = initial spectrum, red = PSS_{365} – 21:79 (**7a-*E*:7a-*Z***).

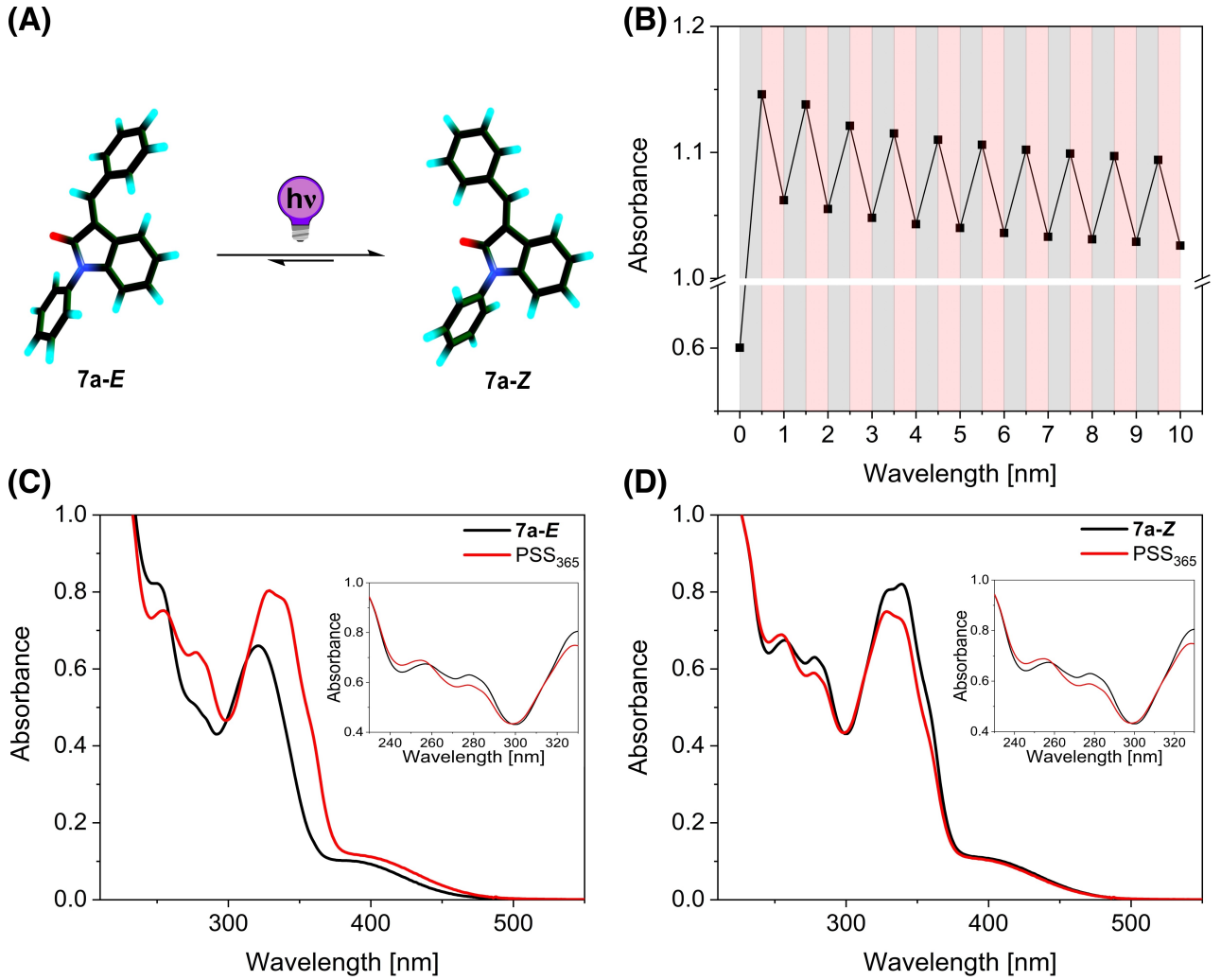

Figure 2. A) DFT optimized structures of **7a-*E*/*Z*** (SMD(CH_3CN)- ωB97X–D/def2-SVP) B) Fatigue study of **7a-*E*** (CH_3CN; 20 °C; 385 and 470 nm LED; change in absorbance at λ = 340 nm; initial jump originates from irradiation towards PSS). UV-Vis spectrum of C) **7a-*E*** and D) **7a-*Z*** (CH_3CN; 20 °C; 365 nm LED) black initial spectrum, red = PSS_{365} (insert shows an enlargement at the isosbestic points).

the same stock solution of **3u-*E*** was first treated with KOH and subsequently with trifluoroacetic acid (TFA), showing that **3u-*E*** can readily be deprotonated and protonated, regaining the same initial absorption spectrum. It is possible at elevated temperatures in an excess of KOH that a retro-Knoevenagel reaction occurs, however this is negligible at room temperature.

Incorporation of molecular switches **3a-*E***, **3d-*E***, **3i-*E***, **3q-*E*** and **3u-*E*** within a biological membrane was achieved by means of thin film hydration and the hydrophobic effect of phospholipids after purification of the samples via size exclusion chromatography (SEC) (method described in Figure S95).[29] Different bilayer synthetic vesicles were created by varying the concentration (5, 10 and 25 mol%) of the corresponding oxindole switch and DOPC (dipalmitoylphosphatidylcholine). The successful formation of 200 nm diameter vesicles containing these molecular switches and their photochemical response was assessed by different characterization techniques and irradiation with a 365 nm LED (Supporting Information, Table S3). Dynamic light scattering (DLS) was used to verify the presence of homogenous vesicles and to obtain their hydrodynamic diameter (D_h, represented by the Z-average) and polydispersity index (PDI). No aggregation for all tested concentrations of the oxindole switches or degradation of the lipid vesicles was observed during the characterization process (same DLS peak maintained as well after irradiation, see Supporting Information). Furthermore, the incorporation of switches at increasing concentrations did not significantly affect the D_h or PDI index indicating good stability, robustness and flexibility of the system. Incorporation of the oxindole switches into the phospholipid membranes was assessed using UV-Vis spectroscopy, by measuring the characteristic absorbance band for each switch, which was successful in all ratios and molecules studied (see Supporting Information, Figure S96–S101).

The prepared samples were irradiated for 1 min with 365 nm light under physiological conditions (PBS buffer, pH 7.4, 37 °C). In Figure 3 A) shows the irradiation of **3a-*E*** in CH_3CN at 20 °C with a 365 nm LED. B) shows the exponential decrease in absorption spectra characteristic of empty liposomes samples.

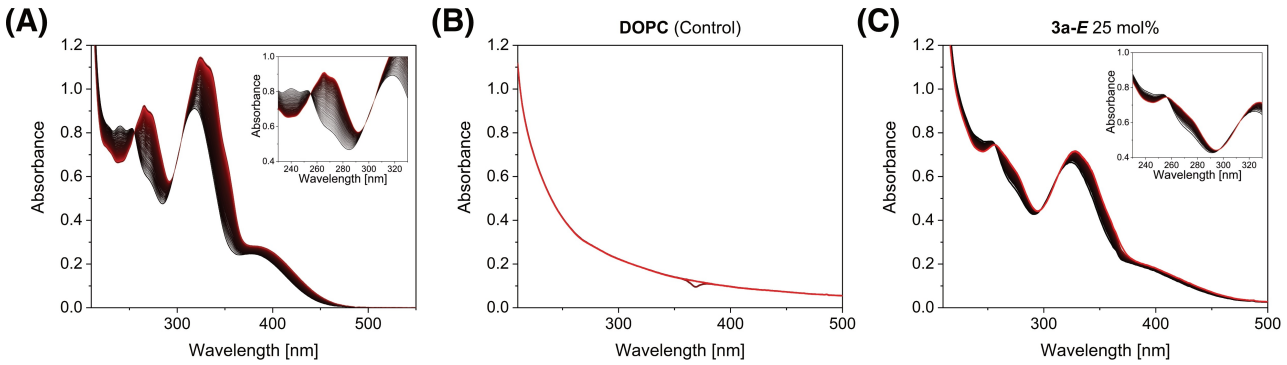

Figure 3. UV-Vis absorption spectrum of A) molecular switch **3a-*E*** (CH_3CN; 20 °C; 365 nm LED), B) DOPC (control) empty liposome and C) liposome-containing 25 mol% oxindole-based molecular switch **3a-*E*** (PBS buffer; 37 °C; 365 nm LED for B) and C); insert shows the isosbestic points as zoom-in).

We also observe no damage to the lipid bilayer when irradiation is performed. C) shows the same irradiation conditions from a sample containing 25 mol% of molecular switch **3a-*E*** (data of other concentrations and switches can be found in the Supporting Information, Figure S96–S101). These results indicate that the studied molecular switches retain their switching effect when incorporated in bilayer membranes. We also observe no destruction of the lipid bilayer after performing the irradiation (DLS peaks remain, Supporting Information), which encourages the use of oxindole molecular switches for further applications in biology and photopharmacology.

Conclusions

To conclude, we designed a new class of photochemically active oxindole-based molecular switches and investigated the photoisomerization processes. These switches are readily accessible in moderate to high yields and all of them show fast and efficient switching behavior in solution, and notably in aqueous buffer while being studied with NMR and UV-Vis. Some of them possessing relatively high quantum yields of up to ~50%, where partial back-switching was observed most distinctively with 470 nm light. The absorbance of **3u-*E*** can be red-shifted by over 50 nm through deprotonation of the hydroxyl group. Switches **3a-*E***, **3d-*E***, **3i-*E***, **3q-*E*** and **3u-*E*** were tested towards their compatibility within synthetic membranes showing distinct switching behavior when incorporated into liposomes verifying them as potential candidates for further applications in drug delivery and photopharmacology.

Experimental Section

Materials and Methods: Chemicals were purchased from commercial sources, by name Sigma-Aldrich, Fluorochem, TCI and used without further purification. Dried solvents were obtained from Acros Organics or from a solvent purification system (MBraun SPS-800). If not stated otherwise, all reactions were carried out in oven-dried crimp top vials under a nitrogen atmosphere using standard Schlenk techniques. Solids were added before crimping the vials and cycled three times between vacuum and nitrogen before addition of liquids. Solutions and reagents were added with nitrogen-flushed disposable syringes/needles. Analytical thin layer chromatography (TLC) was performed on silica gel 60 G/UV265 aluminum sheets from Merck (0.25 mm). Flash column chromatography was performed on silica gel Davisil LC60A (Merck type 9385, 230–400 mesh), a Reveleris X2 Flash Chromatography system from Büchi or a Biotage Selekt system (MPLC) using the indicated solvents. NMR spectra were recorded on a Varian Mercury-Plus 400, a Varian Unity Plus 500 or a Bruker 600 MHz NMR spectrometer at 298 K unless stated otherwise. High resolution mass spectra (HRMS) were recorded on a LTQ Orbitrap XL spectrometer. UV-Vis absorption spectra were recorded on an Agilent 8453 UV-Vis Diode Array System, equipped with a Quantum Northwest Peltier controller in 10 mm quartz cuvettes. Irradiation experiments were performed using LEDs from Thorlabs Incorporated (365, 385, 420 and 470 nm; 0.7 mA for 365, 385 and 420 nm and 1.0 mA for 470 nm).

General Procedure: An oven-dried crimp top vial equipped with a stirring bar was charged with the respective oxindole derivative **2**, **4** or **6** (1.00 equiv.) and aldehyde **1a**–**1u** (1.00 equiv., solid aldehydes). The vial was crimped, flushed with nitrogen and aldehyde **1a**–**1u** (1.00 equiv., liquid aldehydes), dry EtOH (10 mL) and piperidine (80.0 µL) was added. The reaction mixture was heated under continuous stirring at 90 °C for 14–18 h. The reaction mixture was allowed to cool down to room temperature and put on ice. If a precipitate formed, it was filter off using a glass filter frit pore 4, washed with *n*-pentane and dried under reduced pressure. Compounds that did not precipitate were purified via flash column chromatography using a gradient starting from *n*-pentane to CH_2Cl_2 and EtOAc (in case of **3r-*E*** toluene to 10% acetone in toluene).

Supporting Information

The authors have cited additional references within the Supporting Information.[30–36]

Author Contributions

B. L. F. and D. D. conceived the project and designed the molecules. D. D. synthesized, purified and characterized all molecules. D. D. carried out NMR and UV-Vis experiments, and performed DFT calculations. D. R. S. P. and D. D. carried out photochemical quantum yield determination and related data

processing. A. G. carried out studies in biological media. S. C. gave input on quantum yield measurements and DFT calculations. D. D. and D. R. S. P. wrote the manuscript. B. L. F. supervised the work. All authors discussed and commented on the manuscript. S. C. and B. L. F. acquired funding.

Acknowledgements

We thank the Centre for Information Technology of the University of Groningen for providing access to the Peregrine high performance computing cluster. We gratefully acknowledge financial support from the European Research Council (ERC Advanced Investigator grant no: 694345), the Dutch Ministry of Education, Culture and Science (Bonus Incentive Scheme and Gravitation Program no: 024.001.035), the H2020 Excellent Science – Marie Skłodowska-Curie Actions (Innovative Training Network no: 859416 and Individual Fellowship no: 838280) and the Zernike Institute for Advanced Materials at the University of Groningen.

Conflict of Interests

The authors declare no conflict of interest.

Data Availability Statement

The data that support the findings of this study are available in the supplementary material of this article.

Keywords: molecular photoswitches · oxindole · photochemistry · visible light · quantum yields

[1] B. L. Feringa, W. R. Browne, *Molecular Switches*, 2 Vol., Wiley-VCH Verlag GmbH & Co. KGaA, Weinheim, **2011**.
[2] Z. L. Pianowski, *Molecular Photoswitches: Chemistry, Properties, and Applications*, Wiley-VCH Verlag GmbH & Co. KGaA, Weinheim, **2022**.
[3] D. Bléger, S. Hecht, *Angew. Chem. Int. Ed.* **2015**, *54*, 11338–11349.
[4] L. Kortekaas, W. R. Browne, *Chem. Soc. Rev.* **2019**, *48*, 3406–3424.
[5] M. Irie, T. Fukaminato, K. Matsuda, S. Kobatake, *Chem. Rev.* **2014**, *114*, 12174–12277.
[6] A. Goulet-Hanssens, F. Eisenreich, S. Hecht, *Adv. Mater.* **2020**, *32*, 1905966.
[7] Z. Zheng, H. Hu, Z. Zhang, B. Liu, M. Li, D. H. Qu, H. Tian, W. H. Zhu, B. L. Feringa, *Nat. Photonics* **2022**, *16*, 226–234.
[8] Z. Wang, H. Hölzel, K. Moth-Poulsen, *Chem. Soc. Rev.* **2022**, *51*, 7313–7326.
[9] W. A. Velema, W. Szymanski, B. L. Feringa, *J. Am. Chem. Soc.* **2014**, *136*, 2178–2191.
[10] C. Y. Huang, A. Bonasera, L. Hristov, Y. Garmshausen, B. M. Schmidt, D. Jacquemin, S. Hecht, *J. Am. Chem. Soc.* **2017**, *139*, 15205–15211.
[11] C. Petermayer, H. Dube, *Acc. Chem. Res.* **2018**, *51*, 1153–1163.
[12] A. Gerwien, T. Reinhardt, P. Mayer, H. Dube, *Org. Lett.* **2018**, *20*, 232–235.
[13] M. W. H. Hoorens, M. Medved', A. D. Laurent, M. di Donato, S. Fanetti, L. Slappendel, M. Hilbers, B. L. Feringa, W. Jan Buma, W. Szymanski, *Nat. Commun.* **2019**, *10*, 2390.
[14] F. L. Kiss, B. P. Corbet, N. A. Simeth, B. L. Feringa, S. Crespi, *Photochem. Photobiol. Sci.* **2021**, *20*, 927–938.
[15] I. M. Welleman, M. W. H. Hoorens, B. L. Feringa, H. H. Boersma, W. Szymański, *Chem. Sci.* **2020**, *11*, 11672–11691.
[16] D. R. S. Pooler, A. S. Lubbe, S. Crespi, B. L. Feringa, *Chem. Sci.* **2021**, *12*, 14964–14986.
[17] A. D. Marchese, E. M. Larin, B. Mirabi, M. Lautens, *Acc. Chem. Res.* **2020**, *53*, 1605–1619.
[18] a) A. Millemaggi, R. J. K. Taylor, *Eur. J. Org. Chem.* **2010**, 4527–4547; b) R. Kumar, M. M. Alagumuthu, V. Violet Dhayabaran, *J. Heterocycl. Chem.* **2018**, *55*, 1658–1668; c) F. A. Al-Obeidi, K. S. Lam, *Oncogene* **2000**, *19*, 5690–5701; d) W. Delong, W. Lanying, W. Yongling, S. Shuang, F. Juntao, Z. Xing, *Eur. J. Med. Chem.* **2017**, *130*, 286–307.
[19] Y. S. Tingare, M. T. Shen, C. Su, S. Y. Ho, S. H. Tsai, B. R. Chen, W. R. Li, *Org. Lett.* **2013**, *15*, 4292–4295.
[20] J. Wu, J. Chen, H. Huang, S. Li, H. Wu, C. Hu, J. Tang, Q. Zhang, *Macromolecules* **2016**, *49*, 2145–2152.
[21] a) D. Roke, M. Sen, W. Danowski, S. J. Wezenberg, B. L. Feringa, *J. Am. Chem. Soc.* **2019**, *141*, 7622–7627; b) D. R. S. Pooler, R. Pierron, S. Crespi, R. Costil, L. Pfeifer, J. Léonard, M. Olivucci and B. L. Feringa, *Chem. Sci.* **2021**, *12*, 7486–7497; c) D. R. S. Pooler, D. Doellerer, S. Crespi, B. L. Feringa, *Org. Chem. Front.* **2022**, *9*, 2084–2092.
[22] C. Raji Reddy, V. Ganesh, A. K. Singh, *RSC Adv.* **2020**, *10*, 28630–28634.
[23] F. B. Mallory, C. W. Mallory, *Org. React.* **1984**, *30*, 1.
[24] A. V. Marenich, C. J. Cramer, D. G. Truhlar, *J. Phys. Chem. B* **2009**, *113*, 6378–6396.
[25] C. Hansch, A. Leo, R. W. Taft, *Chem. Rev.* **1991**, *91*, 165–195.
[26] A. Corsico Coda, A. Gamba Invernizzi, P. P. Righetti, G. Tacconi, G. Gatti, *J. Chem. Soc. Perkin Trans. 2* **1984**, 615–619.
[27] K. Stranius, K. Börjesson, *Sci. Rep.* **2017**, *7*, 41145.
[28] M. Filatov, M. Olivucci, *J. Org. Chem.* **2014**, *79*, 3587–3600.
[29] D. D. Lasic, *Biochem. J.* **1988**, *256*, 1–11.
[30] S. W. Duan, J. An, J. R. Chen, W. J. Xiao, *Org. Lett.* **2011**, *13*, 2290–2293.
[31] B. Liégault, I. Petrov, S. I. Gorelsky, K. Fagnou, *J. Org. Chem.* **2010**, *75*, 1047–1060.
[32] R. A. Altman, A. M. Hyde, X. Huang, S. L. Buchwald, *J. Am. Chem. Soc.* **2008**, *130*, 9613–9620.
[33] H. J. Kuhn, S. E. Braslavsky, R. Schmidt, *Pure Appl. Chem.* **2004**, *76*, 2105–2146.
[34] M. Montalti, A. Credi, L. Prodi, M. T. Gandolfi, in *Handbook of Photochemistry*, CRC Print, Boca Raton, **2006**.
[35] S. Hoops, S. Sahle, R. Gauges, C. Lee, J. Pahle, N. Simus, M. Singhal, L. Xu, P. Mendes, U. Kummer, *Bioinformatics* **2006**, *22*, 3067–3074.
[36] Gaussian 16, Revision B.01, M. J. Frisch, G. W. Trucks, H. B. Schlegel, G. E. Scuseria, M. A. Robb, J. R. Cheeseman, G. Scalmani, V. Barone, G. A. Petersson, H. Nakatsuji, X. Li, M. Caricato, A. V. Marenich, J. Bloino, B. G. Janesko, R. Gomperts, B. Mennucci, H. P. Hratchian, J. V. Ortiz, A. F. Izmaylov, J. L. Sonnenberg, D. Williams-Young, F. Ding, F. Lipparini, F. Egidi, J. Goings, B. Peng, A. Petrone, T. Henderson, D. Ranasinghe, V. G. Zakrzewski, J. Gao, N. Rega, G. Zheng, W. Liang, M. Hada, M. Ehara, K. Toyota, R. Fukuda, J. Hasegawa, M. Ishida, T. Nakajima, Y. Honda, O. Kitao, H. Nakai, T. Vreven, K. Throssell, J. A. Montgomery, Jr., J. E. Peralta, F. Ogliaro, M. J. Bearpark, J. J. Heyd, E. N. Brothers, K. N. Kudin, V. N. Staroverov, T. A. Keith, R. Kobayashi, J. Normand, K. Raghavachari, A. P. Rendell, J. C. Burant, S. S. Iyengar, J. Tomasi, M. Cossi, J. M. Millam, M. Klene, C. Adamo, R. Cammi, J. W. Ochterski, R. L. Martin, K. Morokuma, O. Farkas, J. B. Foresman, D. J. Fox, Gaussian Inc., Wallingford CT, **2016**.

Manuscript received: May 23, 2023
Accepted manuscript online: June 22, 2023
Version of record online: September 1, 2023